PLASTIC TORSION ON FRICTIONAL JOINTS AND THREE-DIMENSIONAL LIMIT ANALYSIS OF MASONRY STRUCTURES

A.Orduña
University of Minho
Guimarães, Portugal

P. B. Lourenço
University of Minho
Guimarães, Portugal

SUMMARY

The plastic torsion of arbitrarily shaped, frictional joints is established together with its interactions with bending moments and shear forces. In order to solve limit analysis problems, a piecewise linear approximation of the yield function for rectangular joints is proposed. The proposal is incorporated into a model for limit analysis of masonry structures regarded as rigid block assemblages interacting through no tension, frictional joints. An example validates the proposal.

1. INTRODUCTION

The torsion failure in joints can play an important role on the three-dimensional limit analysis of masonry structures. For instance, the out of plane failure of a wall strongly depends on the torsion strength on the bed joints. Bending moments and shear forces on the joint modify its plastic torsion behaviour.

The plastic torsion of beams with arbitrarily shaped cross sections has been soundly established long time ago [7]. Nevertheless, the plastic torsion on frictional joints has been scarcely studied. In [3] Goyal et al. arrive, with a different approach, to the same formulation as presented in section 2 of this paper.

The non-associated limit analysis of three-dimensional masonry structures considered as assemblages of rigid blocks was first formulated by [1], presenting examples only for the associated plasticity case. The torsion model presented in [1] was very simple and approximated. With the same model, [5] presented a solution for a simple example with non-associated flow rules. Nevertheless, the difficulties in obtaining results in agreement with non-linear finite element calculations for more complicated structures motivated a deeper study of the torsion failure mode. The results of this study are summarized in the following sections and a more elaborated example of a wall with out of plane loading is used to validate the model. The work presented here is the extension to three dimensions of that presented earlier for two dimensions in [6].

2. PLASTIC TORSION ON FRICTIONAL JOINTS

Consider an arbitrary shaped joint, Fig. 1a, between two bodies with infinite strength and assume that the no-cohesion Coulomb's law governs the joint's failure. The joint is subjected to a compressive force and to a torsion moment. The origin of the coordinate sys-

tem (x_1, x_2) is located at the centre of twisting. The equilibrium of a differential element dx_1, dx_2 is guaranteed by eq. (1). Here τ_1 and τ_2 are the shear stress components along the axes x_1 and x_2. The yield function is given by eq. (2), where μ is the friction coefficient and σ_n is the applied normal stress. The stress component σ_n is positive in tension, and as no tension stresses are allowed it takes only non-positive values.

$$\frac{\partial \tau_1}{\partial x_1} + \frac{\partial \tau_2}{\partial x_2} = 0 \tag{1}$$

$$\tau_1^2 + \tau_2^2 - (\mu \sigma_n)^2 \leq 0 \tag{2}$$

In the plastic torsion of continuous beams, a boundary condition must be included to force the shear stress to be parallel to the section at the edge [7]. Nevertheless, in the case of a joint, it is possible to think that there exists a strip near the joint edge where the stress directions modify in such a way that they are parallel to the boundary at the very edge. At the limit, when the strip is narrow enough, its influence can be neglected in the calculations. This is possible due to the fact that the infinitely strong adjacent blocks can transmit the resultant stress concentrations. The problem is similar to that of pure plastic shear, where the stress must fall to zero at the very edges that are non-parallel to the action. Under these conditions, it is straightforward to conclude that eq. (3) provides the shear stresses distribution at the joint for the limit torque, represented in Fig. 1b for a rectangular joint. Here θ is the angular polar coordinate. The plastic flow has the same directions as the vector field represented in Fig. 1b with different relative magnitudes.

$$\begin{bmatrix} \tau_1 \\ \tau_2 \end{bmatrix} = \begin{bmatrix} -\sin\theta \\ \cos\theta \end{bmatrix} (-\mu \sigma_n) \tag{3}$$

Under the assumed stress distribution, eq. (4) gives the torsion moment strength, T, of a joint of area S. Here r is the radial coordinate and dA is the area differential. If the centre of twisting (the centre of the stress distribution) is not at the centre of plastic torsion, a shear force resultant exists whose components, V_1 and V_2, are given by eqs. (5) and (6).

$$T = \int_S (-\mu \sigma_n) r dA \tag{4}$$

$$V_1 = \int_S (\mu \sigma_n) \sin(\theta) dA \tag{5}$$

$$V_2 = \int_S (-\mu \sigma_n) \cos(\theta) dA \tag{6}$$

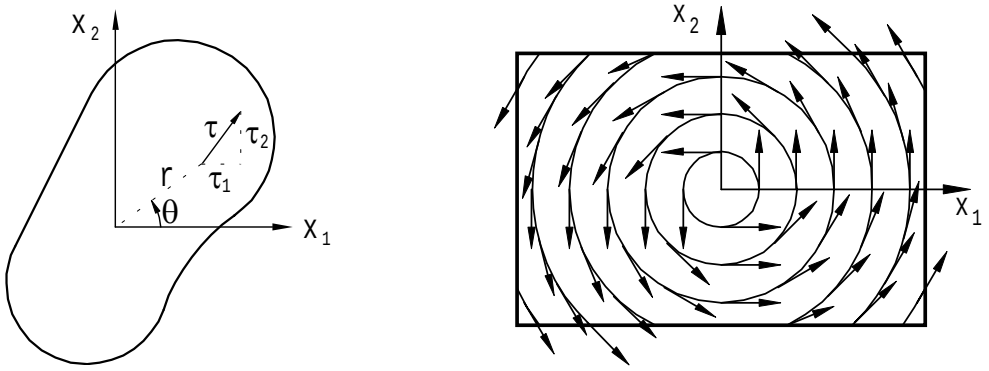

(a) (b)

Figure 1. (a) Joint subject to torsion and (b) stress distribution for a rectangular joint

3. PLASTIC TORSION OF RECTANGULAR JOINTS

In order to perform numerical calculations, eqs. (4-6) can be integrated exactly over a right angled triangle with a vertex at the centre of twisting like that hatched in Fig 2a. For this triangle the integrals of eqs. (4-6) result in the eqs. (7-9). The additional parameters T_1 and T_2 represent the torsion moments produced by the stress components τ_1 and τ_2, respectively; eqs. (10-11) define them and present their expression for the reference triangle. The parameters l_1 and l_2 are defined in Fig. 2a and the constant c is the hypotenuse of the triangle. With these formulae any polygonal shape can be solved just by addition or subtraction of integrals over right-angled triangular areas. Furthermore, the centre of twisting can be placed anywhere, inside or outside the joint.

$$T = \frac{-\mu\sigma_n}{6}\left[l_1 l_2 c + l_1^3 \ln\left(\frac{l_2 + c}{l_1}\right)\right] \tag{7}$$

$$V_1 = \frac{-\mu\sigma_n}{2}\left(l_1 c - l_1^2\right) \tag{8}$$

$$V_2 = \frac{-\mu\sigma_n}{2}\left[l_1^2 \ln\left(\frac{l_2 + c}{l_1}\right)\right] \tag{9}$$

$$T_1 = \int_S -\tau_1 x_2 dA = \frac{-\mu\sigma_n l_1}{6c}\left[l_2^3 + l_1^2\left(l_2 + c\ln\left(\frac{l_2 + c}{l_1}\right)\right)\right] \tag{10}$$

$$T_2 = \int_S \tau_2 x_1 dA = \frac{-\mu\sigma_n}{3}\left[l_1^3 \ln\left(\frac{l_2 + c}{l_1}\right)\right] \tag{11}$$

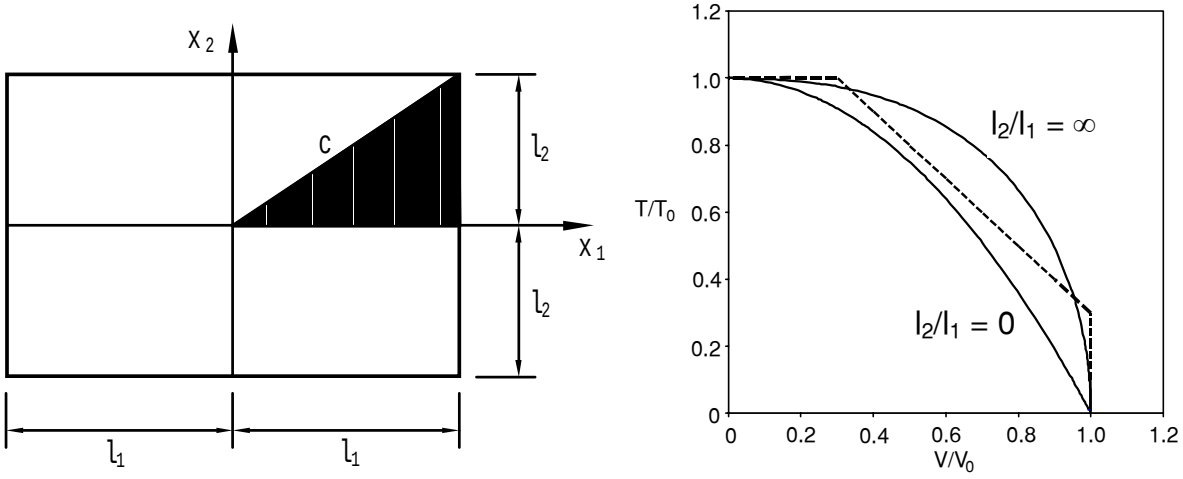

(a) (b)

Figure 2.(a) Rectangular joint; (b) torsion-shear interaction and piecewise linear approximation (in broken line)

In particular, for a rectangular joint as that of Fig. 2a, the limit torque, T_0, is given by eq. (12) in terms of the non-positive normal force at the joint N. Eq. (13) gives the torsion constant, c_T.

$$T_0 = c_T \mu(-N) \tag{12}$$

$$c_{\mathrm{T}} = \frac{1}{3}\left[c + \frac{l_1^2}{2l_2}\ln\left(\frac{l_2 + c}{l_1}\right) + \frac{l_2^2}{2l_1}\ln\left(\frac{l_1 + c}{l_2}\right)\right] \tag{13}$$

If the centre of twisting is moved away from the joint centroid, the interaction between torsion moment and shear force can be studied. Fig. 2b shows two interaction curves for the twisting centre moving along the x_1 axis. The curves represent the extremes of the series that can be obtained for different joint aspect ratios. Defining the aspect ratio as l_2/l_1, the lower curve corresponds to zero aspect ratio and the upper one corresponds to infinite aspect ratio. The remaining curves are in between these two. In the same Fig. 2b a piecewise linear approximation to this family of curves is proposed.

The complete resulting yield functions, φ, are expressed in eqs. (14-18), leading to a total of 26 planes. Eq. (14) constrains the value of the torque while eq. (15) constrains the shear forces along the reference axes; they represent the horizontal and vertical branches in Fig. 2b, respectively. Eq. (16) constrains the shear force along directions at 45º from the reference axes; the vertical branch in Fig. 2b also represents it. Eqs. (17-18) represent the leaning branch on Fig. 2b for shear forces along the reference axes and along 45º rotated axes, respectively. The flow directions are obtained with the associated flow hypothesis but making zero the normal displacement component, so that no dilatancy is present in the model.

$$\varphi_{twist1-2} \equiv \frac{|T|}{c_T} + \mu N \le 0 \tag{14}$$

$$\varphi_{slip1-4} \equiv |V_i| + \mu N \le 0\,;\ i = 1,2 \tag{15}$$

$$\varphi_{slip5-8} \equiv \frac{|V_1| + |V_2|}{\sqrt{2}} + \mu N \le 0 \tag{16}$$

$$\varphi_{V_iT1-4} \equiv \frac{|T|}{c_T} + |V_i| + 1.3\mu N \le 0\,;\ i = 1,2 \tag{17}$$

$$\varphi_{V_{12}T1-8} \equiv \frac{|T|}{c_T} + \frac{|V_1| + |V_2|}{\sqrt{2}} + 1.3\mu N \le 0 \tag{18}$$

The bending moments on a joint, M_1 and M_2, affect the torsion strength by modifying the normal stress distribution. To study this aspect, an additional simplification is required. Here, it is assumed that the normal force on the joint is equilibrated by a uniform stress distribution on a reduced rectangular area. The equilibrium of moments is ensured by shaping this area in such a way that its centroid is located at the point (e_1,e_2), where e_1 and e_2 are the eccentricities of the normal force in the local coordinates system x_1-x_2, see Fig. 3a. Fig. 3b shows the interaction curves obtained for a selected case.

The piecewise linear approximation of this failure mode is a series of planes, that on the first octant contains the points A, B and C of Fig. 3b. It can be shown that these points have the stresses indicated in Table 1. Eq. (19) is the mathematical expression of the corresponding yield conditions and represents a total of eight planes. The flow directions consist of a rotation about the (e_1,e_2) point with the same direction as the torsion moment.

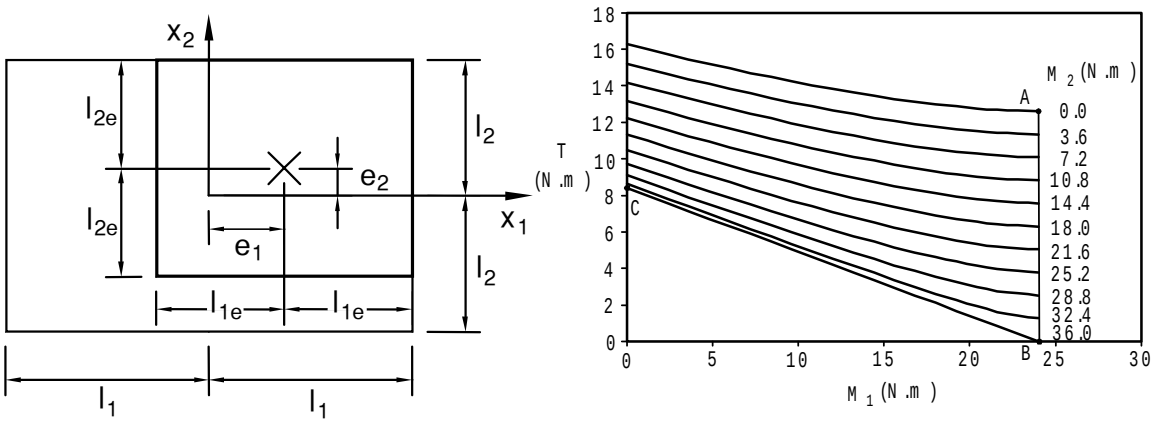

(a) (b)

Figure 3. Torsion-bending moment interaction (a) effective rectangular area and (b) interaction curves for l_1 =0.15 m, l_2 =0.10 m, μ=0.7 and σ_n=4.0 kN/m^2

Table 1. Key stress states for torsion-bending moment interaction

	M_1	M_2	T
Point A	$-l_2N$	0	$-\mu\, l_1N/2$
Point B	$-l_2N$	$-l_1N$	0
Point C	0	$-l_1N$	$-\mu\, l_2N/2$

$$\varphi_{M_{12}T1-8} \equiv \frac{|T|}{l_1+l_2} + \frac{\mu}{2}\left(\frac{|M_1|+|M_2|}{l_1+l_2}\right) + \frac{\mu}{2}N \le 0 \tag{19}$$

4. THREE-DIMENSIONAL LIMIT ANALYSIS OF RIGID BLOCK ASSEMBLAGES

Eqs. (20-25) are the conditions that a limit analysis solution with non-associated flow rule must fulfil, see e.g. [6]. Eq. (20) combines the compatibility and flow rule conditions. Here the columns of the matrix $\mathbf{N}_0$ contain the flow directions for each one of the yield functions in the structure; the flow multipliers for each one of such yield functions form the $\delta\boldsymbol{\lambda}$ vector; $\mathbf{C}$ is the compatibility matrix and $\delta\mathbf{u}$ is the vector of block displacement rates. Eq. (21) is a scaling condition for the displacement rates that ensures the existence of non-zero but finite values. Here $\mathbf{F}_v$ is the vector of variable loads. Eq. (22) ensures equilibrium. Here $\mathbf{F}_c$ is the vector of constant loads; α is the load factor that measures the amount of the live loads that can be applied to the structure at collapse and $\mathbf{Q}$ is the vector of generalised stresses at the joints. Eq. (23) guaranties that the yield functions, vector $\boldsymbol{\varphi}$, are not violated and eq. (24) ensures that plastic flow implies energy dissipation. Finally, eq. (25) guaranties that plastic flow cannot occur unless the stresses have reached the yield surface. Details about these vectors, matrices and functions have been given elsewhere [5]. The modification proposed here is the substitution of the torsion yield functions for eqs. (14-19) as well as the corresponding yield directions.

$$\mathbf{N}_0\delta\boldsymbol{\lambda} - \mathbf{C}\delta\mathbf{u} = \mathbf{0} \tag{20}$$

$$\mathbf{F}_v^T\delta\mathbf{u} - 1 = 0 \tag{21}$$

$$\mathbf{F}_c + \alpha\mathbf{F}_v - \mathbf{C}^T\mathbf{Q} = \mathbf{0} \tag{22}$$

$$\boldsymbol{\varphi} \le \mathbf{0} \tag{23}$$

$$\delta\boldsymbol{\lambda} \geq \mathbf{0} \tag{24}$$

$$\boldsymbol{\varphi}^T \delta\boldsymbol{\lambda} = 0 \tag{25}$$

5. VALIDATION

As a validation example, a wall subjected to out of plane loading is presented. Given the difficulty to find adequate experimental results in the literature, the finite element method has been used to obtain information on collapse modes and collapse load values.

The adopted wall, presented in Fig. 4a, is constrained to horizontal displacements at the left edge. The self-weight acts over the wall as well as variable out of plane body forces proportional to the weight. The structure is 1.053 m high, 0.630 m wide and 0.071 m thick, being the block dimensions equal to 0.081 (height) × 0.210 (length) × 0.071 (thickness) m^3. The volumetric weight is 20 kN/m^3, the friction coefficient is 0.7 and an infinite compressive strength is assumed.

The limit analysis results are compared against a FEM model with the same characteristics. In the FEM model the blocks were modelled with 20 nodes brick elements joined with 16 nodes interface elements. The elastic properties used were: Young's modulus 1.0×10^3 N/mm^2 and Poisson ratio 0.2 for the blocks; normal stiffness 2.4×10^3 N/mm^3 and tangential stiffness 1.0×10^3 N/mm^3 for the interface elements. A Coulomb friction model with zero cohesion and zero dilatancy, available at the DIANA finite element package [2], is adopted for the non-linear analysis.

Fig. 4b present the failure mechanism obtained by the FEM, while Fig. 4c show the limit analysis failure mechanism, both from a back view. These mechanisms are not exactly the same; nevertheless, they are similar and it is well known that masonry structures are prone to exhibit similar slightly different failure modes at close collapse load values [4]. In both mechanisms, two diagonal *yield lines* can be clearly identified: the first going from the bottom of the free edge to the sixth row in the constrained edge, and the second one going from here to the second row from the top on the free edge. These lines divide the wall into three individual regions. The lower region does not move at all. The second region rotates over the first yield line and remains almost as a rigid block. And the top region rotates over the second yield line and over the constrained edge, but also presents internal rotations. These internal rotations are evidenced by the different openings of the head joints from one side of the wall to the other and are more clearly present in the FEM graph than in the limit analysis one, in which sliding effects become clearer. The FEM load factor is 0.210 and the limit analysis one is 0.216. This confirms the good agreement between the results of the two methods.

A key remark must be made here about the solution procedure. The set of eqs. (20-25) has, in general, no unique solution when the flow rules are non-associated. If the load factor is minimised, as proposed by [1], the solution can severely underestimate the failure load factor. The solution presented here was obtained by the following procedure: (1) the equilibrium solution, eq. (22), for only permanent loads (α=0) is obtained minimising the sum of the squared stresses; (2) a solution for the whole set of eqs. (20-25) is obtained for a small compressive effective stress and the load factor is minimised; (3) solutions are computed for successively raising compressive effective stresses; and (4) when no changes are observed between successive solutions, the effective stress is taken as infinity and the final solution is obtained. This procedure aims at introducing the effect of history of loading, i.e.

permanent loads are applied first and variable loads are applied afterwards. Using the standard procedure of [1], the load factor obtained with limit analysis is unrealistic, 0.127, and the failure mechanism obtained is very different from the previous ones; see Fig. 4d. The solution procedure proposed is not intended to be the right one but it has the additional advantage of providing an insight of the failure mechanism development.

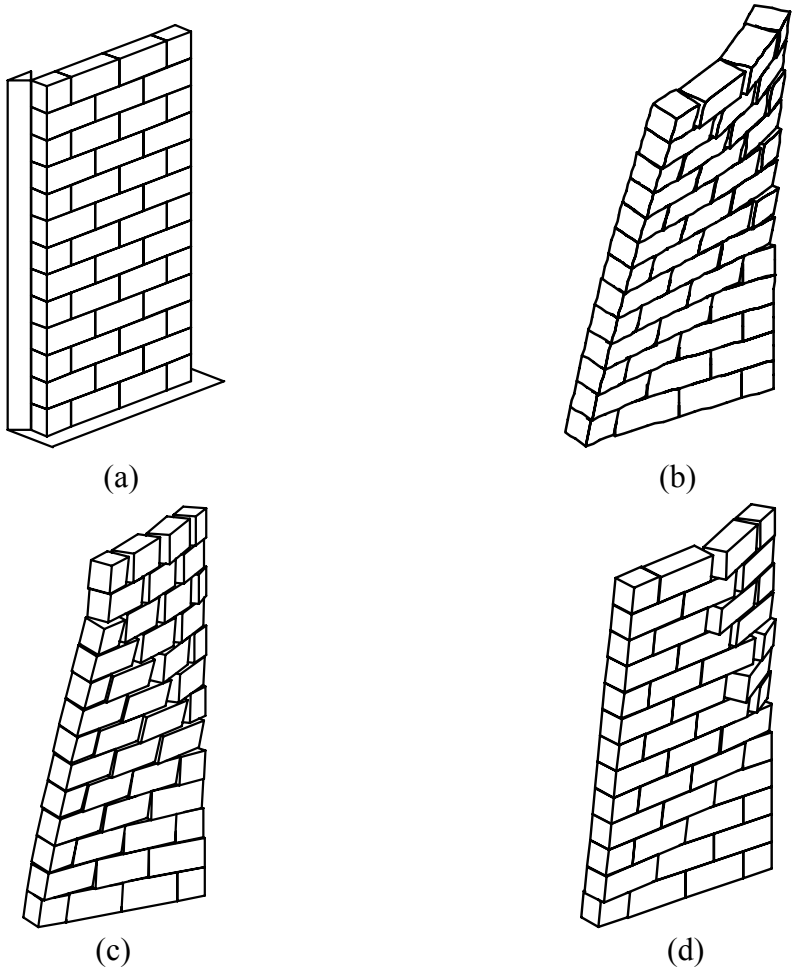

Figure 4. Masonry wall with out of plane loading; (a) model; (b) FEM failure mechanism; (c) limit analysis failure mechanism and (d) wrong failure mechanism

6. CONCLUSIONS

The plastic torsion of frictional joints has been studied and a piecewise linear approximation is proposed. This proposal allows eliminating a possible source of error in the three-dimensional limit analysis of structures modelled as rigid block assemblages. The fact that good results can be obtained for a structure with complex behaviour validates the proposed model.

The question remains regarding the way in which the solution must be calculated due to the multiplicity of solutions for the limit analysis formulation with non-associated flow rules, as unrealistic solutions can be found due to the lack of loading history. The procedure adopted by the authors seems to provide adequate solutions but this topic must be further investigated.

ACKNOWLEDGEMENTS

The first author wishes to thank the scholarship made available to pursue his PhD studies by the Consejo Nacional de Ciencia y Tecnología of Mexico. The work was also partially supported by project SAPIENS 33935-99 funded by Fundação para a Ciência e Tecnologia of Portugal.

REFERENCES

1. BAGGIO, C. and TROVALUSCI, P.
Limit analysis for no-tension and frictional three-dimensional discrete systems, Mechanics of Structures and Machines, Vol. 26, no. 3, 287-304 (1998).
2. DIANA User's Manual Release 7.2
TNO Building and Construction Research, Delft, The Netherlands, 1999.
3. GOYAL S., RUINA A. and PAPADOPOULOS J.
Planar sliding with dry friction, part 1, limit surface and moment function, Wear, Vol. 143, no. 2, 307-330 (1991).
4. LOURENÇO, P. B.
Sensitivity analysis of masonry structures, Proc. 8th Canadian Masonry Symp., Jasper, Canada, 563-574 (1998)
5. ORDUÑA, A. and LOURENÇO, P. B.
Análisis límite en 3D con flujo no-asociado y compresión limitada de estructuras históricas de mampostería, V Congreso de Métodos Numéricos en Ingeniería y Ciencias Aplicadas, Madrid, June 3-6, paper 223 (2002).
6. ORDUÑA, A. and LOURENÇO, P. B.
Cap model for limit analysis and strengthening of masonry structures, J. Struct. Eng. Vol. 129, no. 10, to be published (2003)
7. NADAI, A. – Theory of Flow and Fracture of Solids (2nd ed.) Vol. 1, Chapter 35
McGraw-Hill, New York, 1950.